Published in : Journal of Molecular Medecine (2020), vol. 98, pp. 1737–1751
DOI: 10.1007/s00109-020-01994-9
Status : Postprint (Author's version)

PYRUVATE DEHYDROGENASE KINASE/LACTATE AXIS: A THERAPEUTIC TARGET FOR NEOVASCULAR AGE-RELATED MACULAR DEGENERATION IDENTIFIED BY METABOLOMICS

Vincent Lambert[1,2], Sylvain Hansen[2], Matthieu Schoumacher[3], Julie Lecomte[2], Justine Leenders[3], Pascale Hubert[4], Michael Herfs[4], Silvia Blacher[2], Oriane Carnet[2], Cassandre Yip[2], Pierre Blaise[1], Edouard Duchateau[1], Bénédicte Locht[1], Michèle Thys[1], Etienne Cavalier[5], André Gothot[6], Bernadette Govaerts[7], Jean-Marie Rakic[1], Agnès Noel[2], Pascal de Tullio[3]

1. *Department of Ophthalmology, University Hospital of Liège, Liège, Belgium*
2. *Laboratory of Tumor and Development Biology, GIGA, Université de Liège, Liège, Belgium*
3. *Center for Interdisciplinary Research on Medicines, Metabolomics Group, Université de Liège, Liège, Belgium*
4. *Laboratory of Experimental Pathology, GIGA, Université de Liège, avenue Hippocrate, Liège, Belgium*
5. *Department of Medical Chemistry, University Hospital of Liège, Liège, Belgium*
6. *Department of Hematology and Immuno-Hematology, University Hospital of Liège, Liège, Belgium*
7. *Institute of Statistics Biostatistics and Actuarial Sciences, Université Catholique de Louvain, Louvain-la-Neuve, Belgium*

Vincent Lambert, Sylvain Hansen and Matthieu Schoumacher contributed equally to this work.
Agnès Noel and Pascal de Tullio equally supervised this paper

Abstract

Neovascular age-related macular degeneration (nAMD) is the leading cause of blindness in aging populations. Here, we applied metabolomics to human sera of patients with nAMD during an active (exudative) phase of the pathology and found higher lactate levels and a shift in the lipoprotein profile (increased VLDL-LDL/HDL ratio). Similar metabolomics changes were detected in the sera of mice subjected to laser-induced choroidal neovascularization (CNV). In this experimental model, we provide evidence for two sites of lactate production: first, a local one in the injured eye, and second a systemic site associated with the recruitment of bone marrow–derived inflammatory cells. Mechanistically, lactate promotes the angiogenic response and M2-like macrophage accumulation in the eyes. The therapeutic potential of our findings is demonstrated by the pharmacological control of lactate levels through pyruvate dehydrogenase kinase (PDK) inhibition by dichloroacetic acid (DCA). Mice treated with DCA exhibited normalized lactate levels and lipoprotein profiles, and inhibited CNV formation. Collectively, our findings implicate the key role of the PDK/lactate axis in AMD pathogenesis and reveal that the regulation of PDK activity has potential therapeutic value in this ocular disease. The results

indicate that the lipoprotein profile is a traceable pattern that is worth considering for patient follow-up.

Key messages

- Lactate and lipoprotein profile are associated with the active phase of AMD and CNV development.
- Lactate is a relevant and functional metabolite correlated with AMD progression.
- Modulating lactate through pyruvate dehydrogenase kinase led to a decrease of CNV - progression.
- Pyruvate dehydrogenase kinase is a new therapeutic target for neovascular AMD.

Keywords : Neovascular AMD, Metabolomics, Inflammation, Angiogenesis, Therapeutic target, Lactate

Introduction

Age-related macular degeneration (AMD) is the leading cause of vision impairment in the elderly, in the Western world [1]. Clinically, AMD is classified into early asymptomatic retinal abnormalities, an intermediate form, and two advanced forms associated with severe visual impairment: “dry” AMD (or geographic atrophic form) and neovascular/exudative AMD (nAMD or “wet” AMD). The nAMD is the most severe form of this pathology and the major cause of blindness in people over 50 years old. Choroidal neovascularization (CNV), the hallmark of nAMD, results in the formation of immature and fragile blood vessels causing exudates in the sub-retinal spaces. In the clinics, optical coherence tomography (OCT) examination can monitor disease activity (i.e., the presence of intraretinal and sub-retinal fluids) [2, 3]. Numerous studies have established age, lifestyle, and genetic predispositions as key risk factors for AMD [4–6]. The disease is characterized by a low-grade/subclinical degree of inflammation termed “para-inflammation” [7]. Several cytokines, such as IL-1b [8], IL-18 [9], and IL-33 [10], have been implicated in immune and vascular responses. Moreover, altered cholesterol homeostasis and higher concentrations of high-density lipoproteins have been linked to AMD [11]. Despite these advances, a comprehensive understanding of the pathogenesis and the evolution of this complex multifactorial disease remains incomplete.

The intravitreal administration of anti-vascular endothelial growth factor (anti-VEGF) drugs such as bevacizumab (Avastin®, Genentech), ranibizumab (Lucentis®, Novartis), and aflibercept (Eylea®, Regeneron Pharmaceuticals) represents the cornerstone of the current treatment for patients with nAMD [12, 13]. Non-response to those drugs occurs in up to 21% of eyes [14, 15]. Non-responders to a specific anti-VEGF compound might benefit from a switch to an alternative anti-VEGF drug [14, 15]. Currently, patient follow-up mainly relies on ophthalmologic exams [16] and crucially lacks powerful tools for unbiased biological analyses. Furthermore, the identification of novel therapeutic targets is mandatory to overcome resistance to anti-VEGF treatments.

Metabolomics, defined as the comprehensive identification and quantification of low molecular weight endogenous metabolites in biological samples, offers new opportunities to obtain innovative insights into pathologies and to identify biomarkers/patterns that could be helpful for personalized medicine and improve patient care [17, 18]. Directly linked to the phenotype, this approach provides unique challenging opportunities to correlate dynamic variations in the metabolome with pathological disease status (occurrence and progression) and/or to identify metabolites that are markers and/or key players of the disease [17, 19]. Notably, recent studies have highlighted the implication of metabolism and some energetic metabolites in inflammation and angiogenesis, two identified processes involved in CNV development [20, 21]. In this context, metabolomics has emerged as a relevant tool to obtain new insights into nAMD development through experimental and clinical approaches. Nevertheless, in comparison with other omics sciences, only a small number of metabolomics studies applied to different stages of AMD have been reported [22]. Most of them, based on a mass-spectrometry approach, identified relevant markers and putative biochemical pathways that could be implied in this pathology, mainly in lipid and energetic metabolism [23–25]. Studies using nuclear magnetic resonance (NMR)–based metabolomics are scarce and report small differences between AMD stages [26]. None of those studies has combined a metabolomics screening with an experimental study with the aim of establishing the functional impact of an identified metabolite/marker that could lay down the foundation for novel therapeutic approaches.

Here, we report a NMR-based metabolomics analysis applied to the sera of mice subjected to laser-induced CNV and to serum samples of patients with nAMD. In both experimental and clinical settings, alterations in lactate levels and lipoprotein profiles were detected. Laser-induced CNV [27] was used to mechanistically explore the functional implication of the pyruvate dehydrogenase kinase (PDK)/lactate axis, which is a targetable pathway to modulate the lactate levels [28, 29]. The exciting discovery of lactate as a functional and targetable molecule and the lipoprotein profile as a traceable pattern opens new perspectives for optimizing AMD treatment and patient follow-up.

Methods

PATIENT SELECTION

The study population consisted of unrelated European-Caucasian individuals (> 59 years old) affected with nAMD (n = 72) and healthy volunteers without signs of macular disease or a known family history of AMD (n = 50). Patients with AMD and volunteers were not matched for age or sex. Trained ophthalmologists examined all patients with nAMD and divided them into clinically active or inactive subgroups depending on the presence or absence of intraretinal or sub-retinal exudative fluids as assessed by OCT, respectively. A complete medical history of each patient was obtained by using a standardized questionnaire (i.e., lifestyle, pathologies, treatments, BMI, etc.). Patients and volunteers with diabetes mellitus were excluded from the cohort, while those under treatment for hypercholesterolemia and hypertension were accepted.

BLOOD SAMPLE COLLECTION

For all the participants, peripheral blood was collected after ophthalmological exams in: (1) K_2 EDTA blood collection tubes for blood cell counts, leucocyte differential, and C-reactive protein (CRP) measurement using CRPLX kit (Cobas®, Roche/Hitachi); (2) serum-separating tubes (Greiner); and (3) sodium fluoride/oxalate tubes (Greiner) for the lactate quantification. Serum samples were routinely taken in the morning with a fasting period of at least 2 h. Samples were treated according to clinical standard processes and stored at − 80 °C after sampling until the metabolomics analysis. Clinical biology analyses (lactic acid, CRP, red and white blood cells) were also performed on the sera in order to evaluate patient inflammatory status.

LASER-INDUCED CHOROIDAL NEOVASCULARIZATION IN MICE

CNV was induced in 8-week-old C57BL/6J mice by laser burns as previously described (*n* = 4 to 6 mice per experimental group, minimum 4 impacts per eye) [27]. Mice developing cataracts were excluded from further analyses [27]. Dichloroacetic acid (DCA) was provided in the drinking water according to a described protocol [30]. After measuring the average volume of water consumed by mice every day, the DCA concentration in the drinking water was determined to achieve a daily dose of 3 mg/mouse per day (150 mg/kg/day). At mouse sacrifice, the posterior segments of enucleated eyes were flat-mounted for immunostaining or treated with collagenase for FACS analyses. For CNV quantification, we used FITC-dextran-labeled flat-mounted choroids, as described [27]. In some assays, intravitreous injection of saline or Avastin solution (2 µl −50 µg Avastin/eye) was performed immediately after laser induction, during anesthesia. All animal experiments were approved by the Animal Ethics Committee of the University of Liège.

^{1}H-NMR SPECTROSCOPY AND POST-TREATMENT OF SPECTRA

All samples were recorded at 298 K on a Bruker Avance spectrometer operating at 500.13 MHz for the proton signal acquisition. The instrument was equipped with a 5-mm TCI cryoprobe with a Z-gradient. Maleic acid was used as an internal standard for quantification and trimethylsilyl-3-propionic acid-d4 (TMSP) was used for the zero calibration. Human sera (500 µl) were mixed with D_2O phosphate buffer (100 µl) (0.1 M, pH 7.4), a 35 mM solution of maleic acid (100 µl) (Aldrich, Germany), and TMSP (30 µl) (sodium trimethylsilyl[2,2,3,3-D_4]propionate) in D_2O (10 mg/ml). Mouse sera (200 µl) were mixed with D_2O phosphate buffer (400 µl) (0.1 M, pH 7.4), 35 mM solution of maleic acid (100 µl), and TMSP (30 µl) in D_2O (10 mg/ml). For analyses on other organs, samples were weighed (liver, spleen) or cells were counted (bone marrow) to normalize data (per mg or cell). Samples were prepared as previously described [31].

^{1}H-NMR spectra were acquired using a 1D-CPMG (Carr-Purcell-Meiboom-Gill) relaxation-editing sequence with presaturation for serum samples. The CPMG experiment used a RD-90-(t-180-t)n-sequence with a relaxation delay (RD) of 2 s, a spin echo delay (*t*) of 400 ms, and the number of loops (*n*) equal to 80. The water suppression pulse was placed during the RD. The number of transients was typically 32. The acquisition time was set to 3.982555 s, and a quantity of four dummy scans was

chosen. Data were processed with the Bruker Topspin 3.1 software with a standard parameter set. Phase and baseline corrections were performed manually over the entire range of the spectra, and the δ scale was calibrated to 0 ppm using the internal standard TMSP.

METABOLOMICS ANALYSES

Optimized ^{1}H-NMR spectra were automatically baseline-corrected and reduced to ASCII files using AMIX software (version 3.9.14; Bruker). The spectral intensities were normalized to total intensities and reduced to integrated regions of equal width (0.04 ppm) corresponding to the 0.5–10.00 ppm region. Because of the residual signals of water and maleic acid, regions between 4.7 and 5 ppm (water signal) and 5.6 and 6.2 ppm (maleic acid signal) were removed before analysis. The reduced and normalized NMR spectra were imported to SIMCA (version 14.1, Umetrics AB, Umea Sweden). Pareto scaling was applied to bucket tables, and discriminant analysis (DA), such as principal component analysis (PCA), partial least squares discriminant analysis (PLS-DA), and orthogonal partial least squares discriminant analysis (OPLS-DA), was performed. SIMCA was used to generate all PCA, PLSDA, and OPLS-DA models and plots. Unsupervised multivariate analysis (PCA) was first used to determine intrinsic clusters within the data set, while PLS-DA maximized the separation and OPLS-DA facilitated the graphic visualization of differences and similarities between groups. The quality of OPLS-DA models was determined by the goodness of fit (R^2), and the predictability was calculated on the basis of the fraction correctly predicted in one-seventh cross-validation (Q^2). This workflow was applied for both human and mouse serum samples.

LIPOPROTEIN PROFILE ^{1}H-NMR ANALYSIS

Estimation of lipoprotein profile modification among spectra collected from patients and mice was performed by using peak picking methods that compare intensities between the different fractions. In human and mouse blood NMR spectra, the global signal of lipoproteins between 0.80 and 0.95 ppm is due to an overlap of several peaks that could be linked to the main classes of lipoproteins: very low-density lipoproteins (VLDL), low-density lipoproteins (LDL), intermediary density lipoproteins (IDL), high-density lipoproteins (HDL), and chylomicron. Then, it could be decomposed into distinguishable signals corresponding to these different classes or to a mixture of 2 classes (4 in humans and 5 in mice). To evaluate the proportion of each lipoprotein fraction in the samples, a method based on normalized peak intensity calculation was developed. Then, for each class, we determined the chemical shift corresponding to the peak of signal intensity. For human samples, 4 fractions are selected (F1 = 0.92 ppm (mainly VLDL), F2 = 0.91 ppm, F3 = 0.89 ppm, and F4 = 0.88 ppm (mainly HDL). For mouse samples, 5 fractions are selected (F1 = 0.93 ppm (mainly VLDL), F2 = 0.92 ppm, F3 = 0.90 ppm, F4 = 0.89 ppm, and F5 = 0.88 (mainly HDL)). For each sample, the signal intensity at these different chemical shifts was measured and then normalized to the total intensities of all fractions to reduce the impact of the global lipoprotein concentrations that could differ between samples. Therefore, the obtained values represent a fraction of the total signal. This method allows the comparison between lipoprotein profiles issued from the spectra of blood samples collected from patients with AMD, control subjects, and induced/non-induced mice.

ENZYMATIC AND NMR LACTATE DOSAGES

Enzymatic lactate measurements in whole blood were performed using lactate kit (Cobas®, Roche/Hitachi). NMR lactate quantification was conducted in sera following a described procedure [32].

IMMUNOSTAINING

Flat-mounted posterior ocular poles of mouse eyes were incubated with blocking buffer (PBS containing 10% bovine serum albumin) for 30 min, followed by an overnight incubation, at room temperature with primary antibodies: rat anti-mouse Ly6B.2 (dilution 1:100) (AbDSerotec, MCA771G) or rat anti-mouse Alexa Fluor 647-conjugated F4/80 (dilution 1:100) (Invitrogen, MF48021). To reveal Ly-6B.2 staining, flat-mounted samples were incubated for 1.5 h with a goat anti-rat Alexa Fluor 555-conjugated antibody (dilution 1:1000) (Invitrogen, A-21434). Samples were mounted in Vectashield mounting medium (Vector Laboratories, Burlingame, CA) after washing with PBS. Images were captured with a confocal Leica TCS SP5 microscope using a × 20 objective lens.

BONE MARROW ISOLATION

In some assays, at sacrifice, bone marrow (BM) cells were isolated, as previously described [22], from the tibia and femur of mice subjected or not to laser-induced CNV.

MACROPHAGE ISOLATION IN MOUSE EYE AND STAINING FOR FACS ANALYSIS

After excision, posterior ocular segments were immediately incubated with 2.5 mg/ml collagenase (Sigma) for 1.5 h at 37 °C. The mixture was subjected to mechanical dissociation using a 23G syringe needle and filtered through a 50-µm cell strainer. After FcR blockade with a control isotype (anti-CD16/32, clone R35-95 from BD Biosciences, Erembodegem, Belgium), the immunostaining was performed with the following antibodies: anti-F4/80 (PE, clone BM8, eBioscience, San Diego, CA, USA), anti-CD45 (APC-Cy7, clone 30-F11, eBioscience), and anti-CD206 (APC, clone FAB2535A, R&D systems, Minneapolis, MN, USA). Cell percentages were measured using a FACS Canto II flow cytometer (BD Biosciences) and FACS Diva V 6.1.2 software. $F4/80^{+}/CD206^{-}$ cells were considered M1-like macrophages and $F4/80^{+}/CD206^{+}$ cells were considered M2-like macrophages.

GENERATION OF HUMAN M1/M2 MONOCYTE-DERIVED MACROPHAGES

Human peripheral blood mononuclear cells (PBMCs) were plated overnight in 6-well flat bottom plates (10^7 cells/well) (Nunc, Roskilde, Denmark). The adherent PBMC fraction was grown in complete Roswell Park Memorial Institute (RPMI) medium 1640 containing 50 mM 2-mercaptoethanol and antibiotics (all from Gibco, Merelbeke, Belgium), at 37 °C and 5% CO_2. For macrophage differentiation, monocytes were incubated with M-CSF (100 ng/ml), for 6 days. The M1-like or M2-like polarized macrophages were generated by stimulating cells for 3 days with lipopolysaccharide (LPS) (100 ng/ml) (Sigma-Aldrich, St Louis, MO, USA) and IFN-γ (20 ng/ml) (PeproTech) or IL-4 (20 ng/ml) (ImmunoTools,

Friesoythe, Germany), respectively [33, 34]. In some experiments, lactate or lactic acid (10 mM) was added to M1-like macrophages, for 2 days. Macrophage phenotypes were analyzed through labelling with anti-CD68 (APC, clone Y1/82A, Miltenyi), antiCD80 (FITC, clone L307, BD Biosciences), and anti-CD206 (PE, clone 19.21, BD Biosciences). $CD68^{+}/CD206^{-}/CD80^{-}$ cells were considered M0, $CD68^{+}/CD206^{-}$/CD80+ were considered M1-like, and CD68+/CD206+/$CD80^{-}$ were considered M2-like macrophages. Positive cell percentages were analyzed on a FACS Canto II flow cytometer using FACS Diva software V 6.1.2 (BD Biosciences).

BOYDEN CHAMBER MIGRATION ASSAY

The chemotactic migration of macrophages was evaluated using Boyden chambers (48-well Boyden microchamber; Neuroprobe, Cabin John, MD, USA) and gelatine-coated filters in the presence of serum-containing RPMI [35]. Briefly, lower wells were filled with 27 µl of RPMI medium containing 0.1% bovine serum albumins (BSA) (as a control for random migration) or 1% BSA (as a positive control). Lactate was added at different concentrations (0.1 to 20 mM) to RPMI in the presence of 0.1% BSA. Cell suspension (15 µl) (1×10^{6} cells/ml of RPMI + 0.1% BSA) was added to the upper wells for 5 h at 37 °C. Six wells were used for each experimental condition. One random field/well was counted using an eyepiece with a calibrated grid to evaluate the number of migrating cells.

STATISTICAL ANALYSES

For the in vivo assays, the results related to CNV formation, cell densities, and cell percentages were compared by using a linear mixed model as described [27]. Lactate measurements and Boyden chamber assays were analyzed by using a one-way ANOVA (with Tukey's multiple comparison test), while inflammatory cell quantification was compared by using a two-way ANOVA. For metabolomics studies, unsupervised PCAs and supervised multivariate PLS-DAs and OPLS-DAs were used to discriminate between groups and to identify the main biomarkers (see above in "Metabolomics analyses"). For human and mouse samples, computations were conducted with SIMCA 14.1 software with Pareto scaling of bucket variables.

Univariate statistical analyses were performed on each lipoprotein fraction (see above "Lipoprotein profile ^{1}H-NMR analysis") of both mouse and human serum spectra using GraphPad Prism version 7.0. A nonparametric Kruskal-Wallis test with Dunn's multiple comparison was used to compare Fx controls with Fx AMD patients and Fx mice control versus CNV mice (J5 and J7 post-laser) with Fx being the lipoprotein fraction number 1 to 4 for humans and 1 to 5 for mice.

Hypothesis tests were used to compare AMD cases and controls. *P* values of homogeneity (chi-square or Fisher exact tests) are reported for qualitative variables. For quantitative variables, the *P* values result from one-way ANOVA (parametric or nonparametric (Kruskal-Wallis test) according to D'Agostino and Pearson normality test).

STUDY APPROVAL

The human study was conducted under protocols approved by the Ethical Committee of the University Hospital of Liège, B7072006295 (Belgium). Informed consents were obtained from all study subjects before participation. All animal experiments were approved by the Animal Ethics Committee of the University of Liège.

Results

METABOLOMICS DISCRIMINATES PATIENTS WITH AMD FROM VOLUNTEERS AND ACTIVE PATIENTS FROM INACTIVE PATIENTS

The prospective cohort of patients with and healthy volunteers (Supplemental Table 1) was sub-divided into 3 groups: active AMD (patients with AMD associated with CNV development and exudate), inactive AMD (patients with stabilized AMD without exudate), and healthy donors. Supplemental Table 1 describes patient parameters (sex, age, BMI, clinical biology parameters, treatments). Blood cell counts and C-reactive protein (CRP) measurements were similar in all groups (Supplemental Table 1). However, a slight subclinical increase in monocyte and basophil percentages was noted in patients with active AMD and in patients with inactive AMD compared to healthy volunteers, respectively (Supplemental Table 1). Partial discrimination between all AMD patients (*n*=72) and healthy volunteers (*n*=50) was highlighted by supervised PLS-DAs and O-PLS-DAs of the NMR-based metabolomics spectral data (Fig. 1a). We next focused on the 2 subgroups of AMD patients and noticed also discrimination between patients who are in an active phase (active) and those in a non-active phase (inactive) (Fig. 1b). Importantly, some specific spectral zones and metabolites were responsible for the discrimination of these groups, as shown in the loading plot (Fig. 1c). Increased lactate levels and changes in lipoprotein profiles were linked to the active phase of the pathology (Fig. 1c). Both ^{1}H-NMR (Fig. 1d) and enzymatic (Fig. 1e) dosages in blood samples of patients confirmed increasing lactate concentrations in patients with active AMD, as compared to patients with inactive AMD and healthy volunteers. The NMR signal corresponding to the main different classes of lipoproteins (Fig. 1f) was separated into 4 fractions, namely, F1 to F4, which progressively shifted from a fraction rich in VLDL (F1), to LDL (F2), IDL (F3), and HDL (F4) (Fig. 1g). The analyses of the lipoprotein spectral zone in the 3 patient groups again revealed a shift in the lipoprotein profile. Indeed, both VLDL and LDL (F1 and F2) proportions were higher, while IDL and HDL (F3 and F4) fractions were reduced in the active group compared to inactive and healthy individuals (Fig. 1h).

METABOLOMICS OF MICE SUBJECTED TO CNV LED TO IDENTIFICATION OF CNV-LINKED METABOLITES

When mice were subjected to laser-induced CNV, neovascular lesions appeared at day 5 after induction and were the largest at day 7 (Fig. 2a–d), in agreement with previous reports [12, 27, 36]. Concomitant longitudinal metabolomics analyses performed on blood samples highlighted a good

concordance between CNV occurrence and the evolution of the metabolome patterns observed during the first week following laser burn (Fig. 2e–g). The most significant discrimination between control (CTL) and induced mice occurred at days 5 and 7 post-laser burn when the CNV was detectable on flat-mounted choroids (Fig. 2b, c, f, g). In line with the clinical data generated in the human study, lactate and lipoprotein profiles were the main discriminating metabolites (Fig. 2h–j) between the two experimental groups. Consistently, lactate concentrations measured by NMR were increased by approximately 15% in the blood of laser-induced mice at day 5 (Fig. 2k) ($P < 0.05$). The NMR signal corresponding to the main different classes of lipoproteins (Fig. 2l) was separated into 5 fractions, namely F1 to F5, which progressively shifted from a fraction rich in VLDL (F1), to LDL (F2), to one richest in HDL (F5) (Fig. 2m). The kinetic analysis of lipoprotein profiles revealed that the proportion of LDL/VLDL-containing fractions (mainly F1 and F2) progressively increased, while HDL fractions (mainly F4 and F5) decreased during CNV development (Fig. 2n). Collectively, these data highlight two main discriminant metabolites between control and CNV-induced mice: lactate whose increased levels were detected at day 5, and a shift in the lipoprotein profile (VLDL-LDL/HDL ratio), which was the highest at day 7.

LACTATE HAS A FUNCTIONAL ROLE IN CNV DEVELOPMENT

Lactate is a targetable metabolite whose level can be modulated by interfering with pyruvate dehydrogenase kinase (PDK), which inactivates the pyruvate dehydrogenase (PDH) involved in pyruvate conversion into acetyl-CoA in the mitochondria (Fig. 3a). In the mouse model, PDK activity was blocked by treatment with dichloroacetic acid (DCA) [37]. In line with our expectation, DCA treatment decreased blood lactate levels at day 5 (Fig. 3b) and led to a significant reduction in CNV formation of 46%, at day 7 (Fig. 3c–e). These data demonstrate the functional role of lactate in CNV development. Notably, similar effects on blood lactate levels (Fig. 3g) were observed by using anti-VEGF antibodies (injected intravitreously at day 0), which are highly potent anti-angiogenic agents (Fig. 3f). In line with the clinical data, DCA treatment restored the lipoprotein profiles (Fig. 3h) with a distribution of the fractions similar to that seen under control conditions (lower F1/F2 and higher F4/F5 proportions) (Fig. 3h). Thus, DCA treatment induced a normalization of lipoprotein profiles. Interestingly, anti-VEGF antibodies also modified the lipoprotein profile with reduced VLDL/LDL (F1–F3 fractions) and increased HDL (F4 and F5 fractions) proportions as compared to control mice (Fig. 3i).

LACTATE PRODUCED LOCALLY AND SYSTEMICALLY MODULATES INFLAMMATION AND MACROPHAGE POLARIZATION

To determine the cellular source of lactate detected in the serum at day 5 (Fig. 2k), we conducted NMR dosages in different organs at days 3 and 5 post-laser induction. Increased lactate levels were detected locally in injured eyes as early as day 3 (Fig. 4a). At this time point, no significant modification of lactate levels was detected in the serum (Fig. 2k), bone marrow, spleen, or liver (Fig. 4b–d). Interestingly, at day 5, a substantial increase in lactate levels was noted in the bone marrow (Fig. 4b). Notably, DCA-treated mice displayed normalized lactate levels in eyes at day 3 (Fig. 4a) and in the bone marrow at day 5 (Fig. 4b). A slight decrease of lactate level was seen in spleen after DCA treatment at day 3 (Fig.

4c). These data reveal two sites of lactate production: an early and local production of lactate in the injured eye, followed by a release of lactate in the blood circulation by bone marrow–derived inflammatory cells.

Ly6b2$^+$ neutrophil infiltration occurred at day 1 post-laser burn and then rapidly decreased from days 3 to 7 (Fig. 4e–i), while the F4/80$^+$ macrophage density progressively increased after CNV induction and peaked at day 5 (Fig. 4j–m). Upon DCA treatment, neutrophil recruitment was slightly decreased at day 1 (Fig. 4i). An earlier infiltration of macrophages (Fig. 4n) was observed upon DCA treatment and associated with a 1.85-fold reduction in the percentage of pro-angiogenic M2-like macrophages (CD45$^+$, F4/80$^+$, and CD206$^+$ cells) (Fig. 4o). The impact of lactate on macrophage migration and polarization was next evaluated in vitro. Human peripheral monocytes were first polarized in vitro into M1 or M2 subtypes and then subjected to a lactate gradient in a Boyden chamber assay. Lactate was a potent chemoattractant for M1-like macrophages (at 10 mM and 20 mM) and M2-like macrophages (at 1 and 2 mM) (Fig. 4p, q). We next hypothesized that lactate can repolarize M1-like macrophages into M2 macrophages. To address this issue, macrophages were stimulated with LPS and IFN-γ to polarize them into an M1-like phenotype (Fig. 4r). Under those conditions, approximatively 30% of the macrophage population were M1-like and < 4% were M2-like macrophages. The subsequent addition of lactate for 2 days led to a shift in the macrophage population, which was then composed of approximatively 25% M2-like macrophages and < 2% M1-like macrophages. Collectively, these data reveal that lactate modulates macrophage recruitment and the M1/M2 balance in favor of M2-like macrophages by converting M1 macrophages to M2 macrophages.

DCA IS MORE EFFICIENT DURING THE ANGIOGENESIS PHASE

Our experimental data allowed us to correlate the systemic increase in lactate levels with macrophage recruitment and the angiogenic phase (CNV formation) (Fig. 5a). Interestingly, CNV formation and macrophage recruitment in the eye were concomitant with the increase in lactate levels observed in the bone marrow and in the serum. To define the best therapeutic window for DCA treatment, we designed several treatment schedules to target several steps of disease development: (i) the whole process (D0–D7); (ii) the neutrophilic response (D0–D2); (iii) the initial macrophage recruitment associated with increased local lactate levels (D0–D4); and (iv) the boost of systemic lactate production associated with early (D3–D5) and late (D4–D7) CNV formation (Fig. 5b). CNV inhibition was optimal when DCA treatments were applied during the whole process (D0–D7) (Fig. 5c). In contrast, only a partial CNV impairment was observed upon treatment during earlier periods (D0–D2, D0–D4, and D3–D5). Of note, when we reproduced the clinical situation by applying DCA treatment during the late-angiogenic phase (D4–D7), CNV inhibition was optimal and reached that observed with a treatment applied during the whole process. These findings emphasize the interest of the PDK/lactate axis as a therapeutic target to treat patients with active AMD.

Discussion

The present holistic study highlights that metabolomics is a relevant tool to obtain new insights into nAMD. Here, we assign a functional role for the PDK/lactate axis in AMD and in CNV progression that holds promise for new treatment. Moreover, a shift in the lipoprotein profile towards higher VLDL-LDL proportions was associated with CNV development providing novel markers of pathology progression that could be suitable for patient treatment follow-up and personalized medicine. The clinical relevance of our innovative findings is supported by similar metabolomics changes detected in samples of patients with nAMD and in murine samples in a pre-clinical model.

The most important finding of our human study is the detection of metabolomics differences between patients with active AMD (in an active exudative phase of the pathology) and healthy or non-active patients. This original observation underlines the underappreciated nonlinear features of this chronic disease and reveals that the exudative phase in patients is concomitant with serum changes detectable by metabolomics. Notably, increased serum lactate levels and a shift in the lipoproteins profile (increased VLDL-LDL/HDL ratio) were noted during the active phase of the pathology. Furthermore, the increase in the VLDL-LDL proportion is in line with reported data that associated AMD with a higher level of LDL [38]. Similar metabolic alterations as those seen in the human study (increase in lactate levels and changes in the VLDL profile) were identified in mice during CNV formation. The good correlation between the metabolomics data generated from mouse and human samples validates our concept and also indicates that the animal model correctly reflects the active phase of nAMD [27].

We next focused our investigation on the PDK/lactate axis as a putative therapeutic target for AMD treatment. The implication of lactate in angiogenesis and inflammation, the two underlying causes of AMD, is well documented [39, 40]. However, its role in ocular disease has not yet been reported. In the present study, we provide evidence that lactate controls the recruitment of macrophages, which are well recognized as key cellular regulators of CNV formation [41, 42]. Importantly, the normalization of lactate levels by pharmacological inhibition of PDK in mice modified the kinetics of macrophage recruitment and regulated M1/M2 balance by reducing the percentage of the M2 subtype. M2 macrophages are considered pro-angiogenic cells that contribute to different pathologies including AMD [43, 44]. Our data reveal that lactate can exert direct and differential effects on M1 and M2 macrophage properties. Lactate is a chemoattractant for M1- and M2-like macrophages with different optimal concentrations for each macrophage subtype. Of note, a key finding here is that lactate promotes the repolarization of M1-like to M2-like macrophages. Our observations are in line with a previous study implicating lactate in the M2 macrophage polarization in the context of cancer [45]. Therefore, increasing concentrations of lactate could attract M1 macrophages that can locally repolarize into pro-angiogenic M2-like macrophages. Altogether, our data support the interest of targeting lactate metabolism as a promising approach, not only for cancer [46] but also for AMD.

The source of lactate and its increased levels detected in the serum are intriguing issues. We are providing evidence that the increased lactate levels detected in eyes preceded those in sera. This result supports the local production of lactate at an early stage following eye injury, which can be caused by laser burn in mice and likely by lifelong exposure of the retina and the underlying retinal pigment

epithelium (RPE) to different stimuli (light, oxidative stress) in aging patients. At the cellular level, lactate could be secreted by cells exhibiting aerobic glycolysis, such as RPE [47] and endothelial cells [48]. Hypoxia could also trigger glycolysis and lactate production by resident and inflammatory cells. A progressive enhancement of lactate production was observed in eyes until day 3, excluding neutrophil involvement in this secretion. A very important finding is the increased lactate production observed at day 5, concomitantly in bone marrow extracts and sera. We provide evidence for lactate production in two sites: a local one caused by ocular tissue injury and a systemic one induced by circulating inflammatory cells.

This observed dual production of lactate explains the similarity in metabolomics fingerprints detected in patients with nAMD and in the experimental model, which could be considered intriguing. In the course of AMD, age-related chronic para-inflammation (an intermediate between basal and inflammatory states) occurs in the retinochoroidal tissues [7, 49]. Constant exposition to light stimulation and other oxidative stresses generates large amounts of oxidized materials and reactive oxygen species (ROS) that promote complement activation, cell damage, drusen formation, and irreversible photoreceptor degeneration. Prolonged ROS augmentation, hypoxia, and chronic inflammation can then trigger angiogenic signaling leading to CNV, a hallmark of advanced stage of the disease. In the experimental CNV mouse model, the laser injury induced Bruch's membrane rupture, cell damage, and hypoxia, finally causing CNV formation. Although the events leading to human CNV are clearly different from those in laser-induced trauma, the subsequent angiogenic response that occurs in human CNV due to the breakdown of Bruch's membrane is reproduced in the laser injury model [27]. Thus, the murine laser-induced CNV model reproduces the late events occurring in nAMD progression. This concept is further supported by our following findings: (1) in clinical samples, higher lactate levels and lipoprotein profile shifts are detected in patients with active AMD; (2) in the experimental model, metabolite changes are detected from day 5 in blood and are concomitant to late-inflammatory and angiogenic phases; (3) lactate level normalization through a pharmacological approach is more potent when applied at late (> day 4 post-cauterization) than at early (< day 4) time points; and finally (4) the inhibition of angiogenesis through anti-VEGF antibody administration normalized lactate levels. These observations further support the relevance of the laser-induced CNV model in reproducing the AMD pathology [27].

Of great interest is our finding that lactate levels and lipoprotein profiles are normalized and modified upon anti-VEGF and PDK inhibitor treatments. Our study opens a new horizon for personalized medicine and the follow-up of patients with nAMD during anti-angiogenic therapy. Indeed, to determine the number and frequency of anti-VEGF intravitreous injections, clinical practitioners are currently mostly following general guidelines in the absence of evidence-based methods to guide them. Personalized-based protocols of treatment are not yet available, and tools are lacking for providing a rationale for decision-making and guiding clinicians. In this context, our metabolomics results offer an opportunity to monitor some metabolite levels in biofluids such as lactate and the lipoprotein profiles. The lactate level is followed as a prognostic/predictive marker in cancers [50, 51], and combined with the lipoprotein profile, it could be used for the follow-up of patients with nAMD during anti-angiogenic treatment and/or in order to personalize therapeutic interventions for nAMD.

Moreover, the normalization of lactate levels by oral PDK modulators clearly represents a new therapeutic option and/or a complementary treatment to reduce CNV progression.

In conclusion, our study provides new conceptual insights into the pathogenesis and evolution of poorly understood nAMD and supports the innovative concept of the PDK//lactate axis as a functional, traceable, and targetable mediator of CNV and nAMD progression. In addition to offering a novel therapeutic option for AMD treatments, our work suggests that metabolomics profiling and lactate/lipoprotein level monitoring during treatment are worth considering for the follow-up of patients with AMD in future clinical studies and offer new tools to help clinicians in personalized therapeutic design.

Acknowledgments

We gratefully acknowledge the medical and technical assistance of M. Dumez, N. Marenne, C. Noel, A. Oger, C. Rogister, B. Detry, C. Fink, M. Dehuy, I. Dassoul, P. Roncarati, J. Parotte, J. Lhoest, G. Musso, and C. Benveniste. We thank the GIGA (Groupe Interdisciplinaire de Génoprotéomique Appliquée, University of Liège, Belgium) for the access to the several platforms (GIGA-Imaging and Flow Cytometry platform and GIGA-Mouse facility and Transgenics platform) and the Center for Interdisciplinary Research on Medicines (CIRM) for the access to the NMR-Santé platform.

Authors' contributions

V.L. designed the study, performed the in vivo experiments, collected human and murine data with SH, CY, and J. Lecomte. M.S. and J. Leenders performed the metabolomics studies and analyzed the data. M.H. and P.H. performed the assays using macrophages; S.B. performed the computer-assisted quantifications; O.C. performed the bone marrow isolation; P.B., E.D., B.L., and M.T. contributed to patient recruitment and ophthalmic examinations. E.C. and A.G. performed human blood sample analyses; P.d.T. and B.G. performed statistical analyses on metabolomics assays; J-M.R. contributed to the design of the clinical study, data analyses, and manuscript preparation; A.N. designed and supervised the study, analyzed, and interpreted the experimental data, and P.d.T. designed the project, supervised the study, and performed the metabolomics study. A.N. and P.d.T wrote the manuscript and gathered manuscript modifications from the authors. All authors revised the manuscript.

Funding

This work was supported by grants from the Fonds de la Recherche Scientifique FNRS (F.R.S.-FNRS, Belgium), the Fonds spéciaux de la Recherche (University of Liège), the Fondation Hospitalo Universitaire Léon Fredericq (FHULF, University of Liège), the REGION WALLONNE (Direction Générale Opérationnelle de l'Economie, de l'Emploi et de la Recherche, SPW, Belgium), and the FEDER project No. DMLA-AB/ULG (Fonds européen de développement régional). P. de Tullio is a Research Director of the F.R.S.-FNRS.

Data availability

The metabolomics and all the data reported in this paper are available on demand from the Laboratory of Biology and Tumor Development and the Metabolomics Group of the University of Liège.

Compliance with ethical standards

Competing interests

The authors declare that they no competing interests.

Ethics

Animal experiments were performed in compliance with the Animal Ethical Committee of the Liège University (Liège, Belgium) after the approval of the local Animal Ethical Committee. The human study was conducted under protocols approved by the Ethical Committee of the University Hospital of Liège, B7072006295 (Belgium). Informed consent was obtained from all study subjects before participation.

Code availability

Metabolomics data were processed using Bruker Topspin 3.5 and AMIX 3.9 software. Metabolomics analyses were performed using SIMCA 14.1 software. Statistical analyses were performed using GraphPad Prism 7.0 software.

Electronic supplementary material The online version of this article (https://doi.org/10.1007/s00109-020-01994-9) contains supplementary material, which is available to authorized users.

Figures

Fig. 1 *Lactate and lipoproteins are the main increased discriminant metabolite in serum of patients with nAMD.* ***a*** *Score plot derived from an OPLS-DA of spectral data (3 components, R^2 = 0.527, Q^2 = 0.151) collected from patients with nAMD (blue dots, n = 72) and healthy volunteers (green dots, n = 50). Each data point represents an individual patient.* ***b*** *OPLS-DA score plot (2 components, R^2 = 0.468, Q^2 = 0.21) of spectral data collected from patients with active (red dots, n = 49) and inactive (blue dots, n = 23) nAMD.* ***c*** *Loading plot of spectral data collected from patients with active and inactive nAMD highlighting lactate and lipoproteins as biomarkers of active status.* ***d*** *NMR and* ***e*** *biochemical dosages of blood lactate in the serum of healthy volunteers and patients with active and inactive forms of AMD. Data are expressed as the percentage of healthy donors.* ***f*** *NMR spectrum of human serum highlighting the lipoprotein profiles (from 0.88 to 0.92 ppm).* ***g*** *Enlarged view of the lipoprotein NMR spectral zone showing the chemical shift corresponding to the maximum intensity of the signal of the 4 lipoprotein classes.* ***h*** *Modification of the lipoprotein profile during CNV development. Fraction 1 is mainly composed of VLDL, while fraction 4 is mainly composed of HDL. *P < 0.05; **P < 0.01; ***P < 0.001. Error bars are SEM*

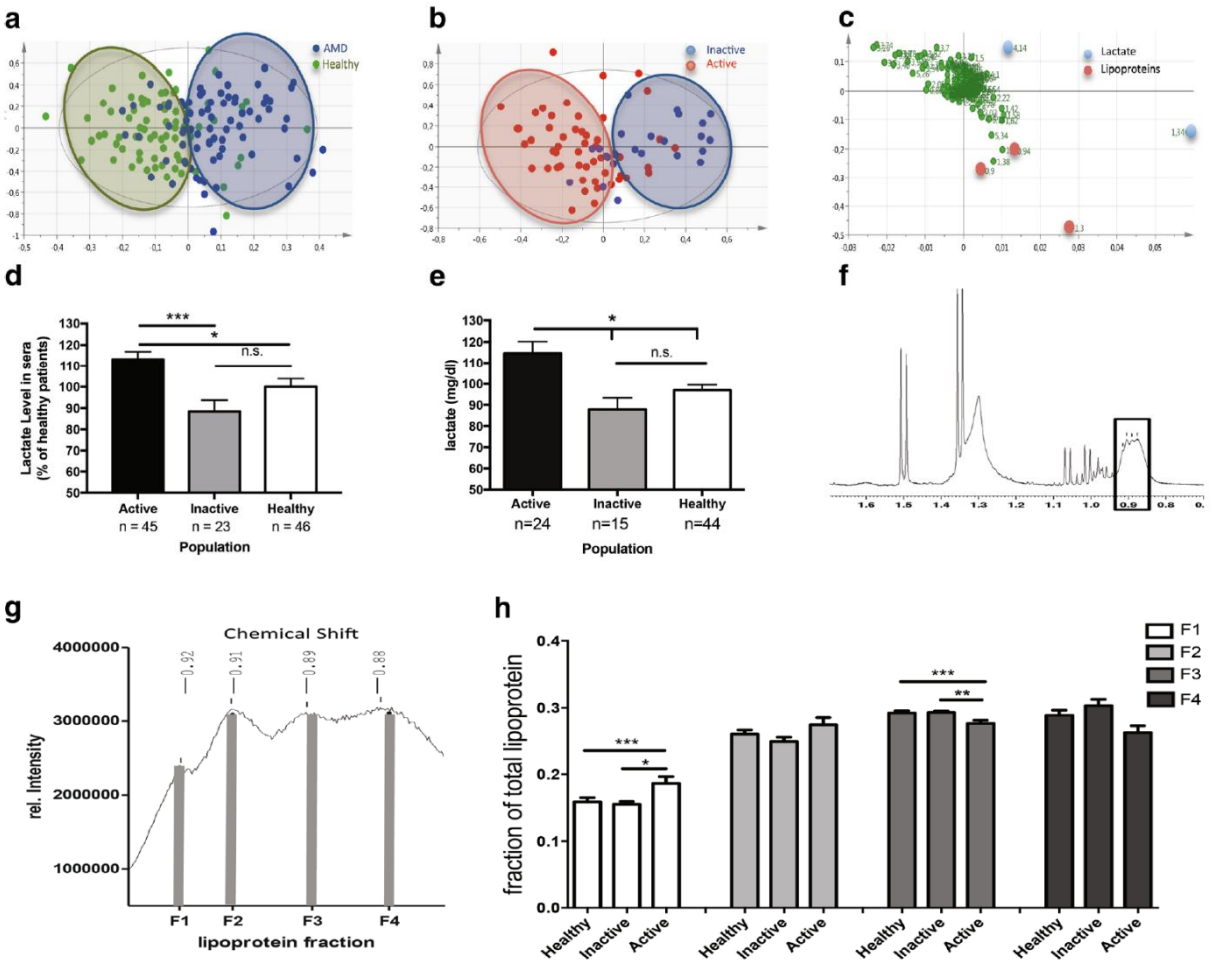

Fig. 2 *Lactate and lipoproteins are the main increased discriminant metabolites in the serum of mice subjected to CNV. Mice were subjected (CNV) or not (CTL) to a laser burn. FITC-dextran-labeled flat-mounted choroid observed at day 3 (**a**), 5 (**b**) or 7 (**c**) after laser induction. Dashed lines delineate the lesion. Scale bars, 100 µm. Quantification of fluorescent neovessel area with ImageJ software (n ≥ 4 mice/group, n ≥ 12 laser impacts/group) at days 1, 3, 5, and 7 (**d**). *P < 0.05; ***P < 0.001. Error bars indicate SEM. Score plot resulting from a PLS-DA analysis of spectral data performed at day 3 (**e**), day 5 (**f**), and day 7 (**g**) after laser induction (control vs J3: 2 components, R^2 = 0.579 and Q^2 = 0.119; control vs J5: 3 components, R^2 = 0.669 and Q^2 = 0.841; control vs J7: 3 components, R^2 = 0.793 and Q^2 = 0.734). Laser-induced mice (green dots) were distinguishable from non-induced mice (blue dots) at day 5 and day 7. Each data point represents an individual mouse (n ≥ 4 mice/group). Loading plot resulting from a PLS-DA analysis of spectral data performed at day 3 (**h**), day 5 (**i**), and day 7 (**j**) after laser induction. Lactate (blue dots) and lipoproteins (red dots) are the main discriminant metabolites. NMR dosage of serum lactate levels at day 7 (n ≥ 5 mice/group) (**k**). The results are expressed as the percentage of the control. *P < 0.05; **P < 0.01. Error bars indicate SEM. NMR spectrum of mouse serum highlighting the lipoprotein profiles (from 0.88 to 0.93 ppm) (**l**). Enlarged view of the lipoprotein NMR spectral zone showing the chemical shift corresponding to the maximum intensity of the signal of the 5 lipoprotein classes (**m**). Modification of the lipoprotein profile during CNV development (**n**). Fraction 1 is mainly composed of VLDL while fraction 5 is mainly composed of HDL (n ≥ 5 mice/group). *P < 0.05; **P < 0.01. Error bars are SEM*

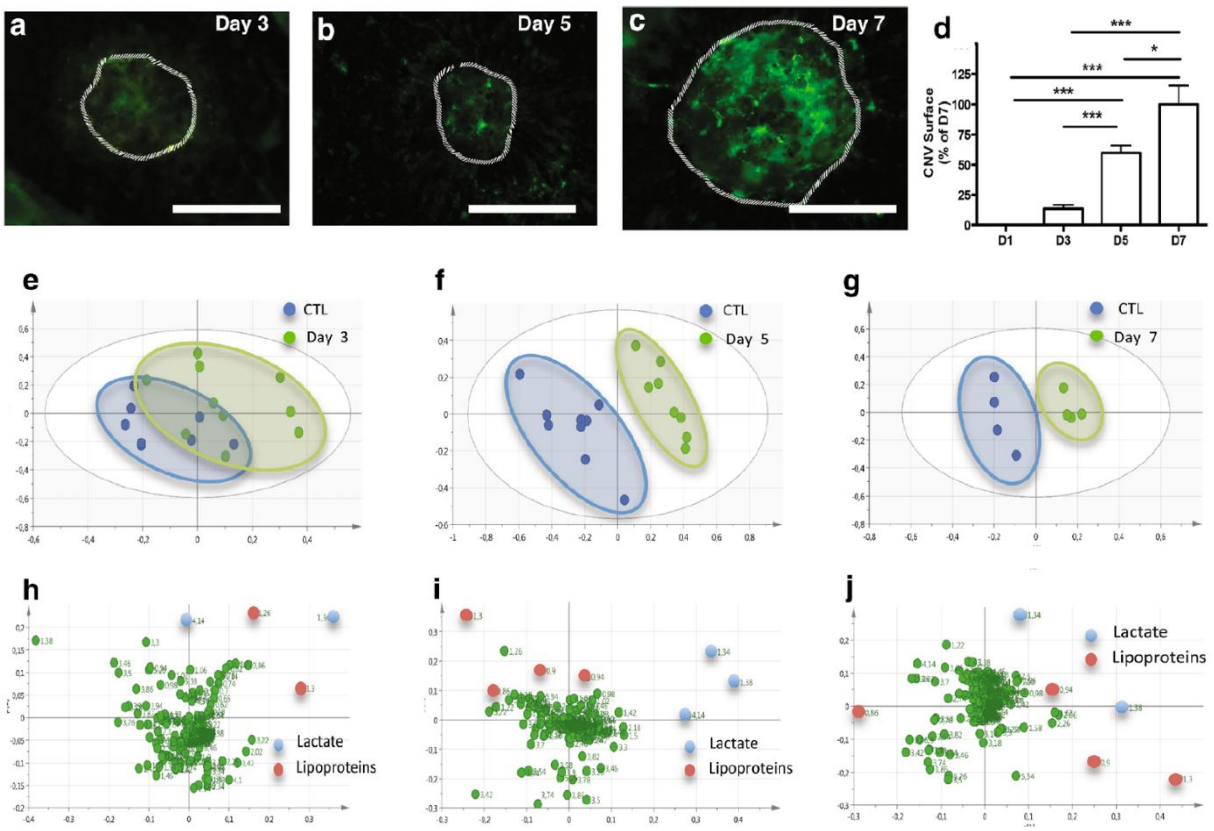

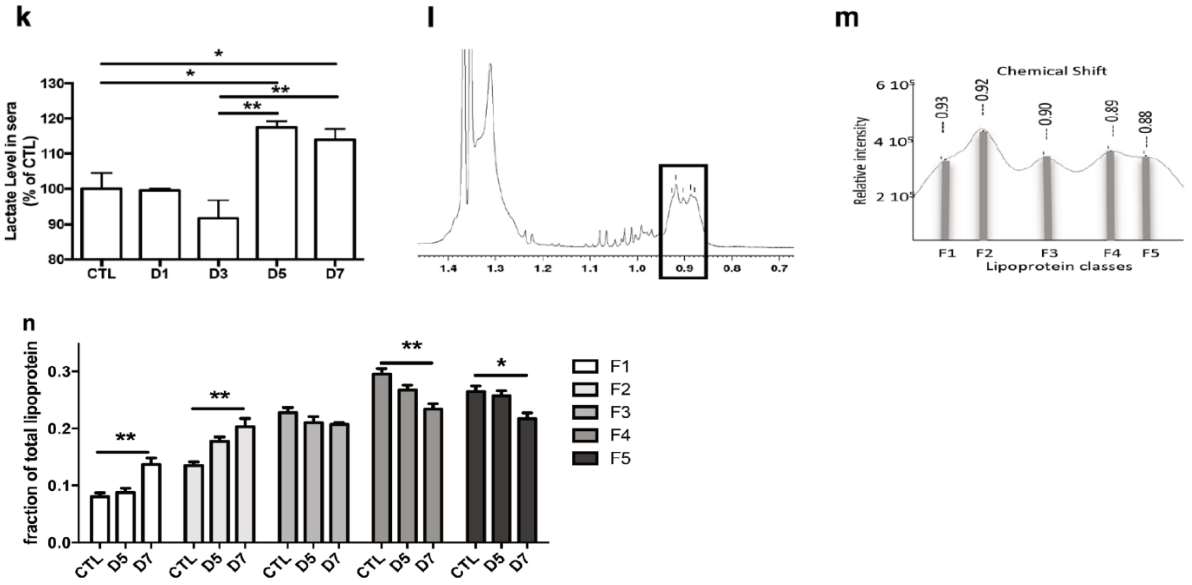

Fig. 3 *DCA treatment normalizes lactate level and reduces CNV surface.* ***a*** *Schematic overview of how DCA can impact lactate levels. DCA inhibits mitochondrial PDK activity, thereby maintaining PDH in its (unphosphorylated) active form and facilitating the decarboxylation of pyruvate to acetyl-CoA. As the flux of pyruvate is accelerated, the equilibrium between lactate and pyruvate is unbalanced towards pyruvate.* ***b–e*** *Mice subjected to laser-induced CNV were treated or not with DCA (3 mg DCA/day/mouse) (n ≥ 5 mice/group). Untreated mice (laser) were used as controls.* ***b*** *NMR dosage of serum lactate level at day 7 after DCA treatment (n ≥ 5 mice/group). The results are expressed as the percentage of laser-induced mice without treatment. *P < 0.05; **P < 0.01. Error bars correspond to SEM. Flat-mounted choroid of* ***c*** *an untreated mouse and* ***d*** *a DCA-treated mouse at day 7: Dashed lines delineate the lesion. Scale bars, 100 µm.* ***e*** *Quantification of CNV after DCA treatment at day 7 (n ≥ 6 mice/group, n = 26–27 laser impacts/group). The results are expressed as the percentage of laser-induced mice without treatment. **P < 0.01. Error bars correspond to SEM.* ***f*** *Quantification of CNV after Avastin treatment at day 7 (n ≥ 6 mice/group, n = 26–27 laser impacts/group). The results are expressed as the percentage of laser-induced mice without treatment.* ***g*** *NMR dosage of serum lactate level at day 7 after Avastin treatment; the results are expressed as the percentage of laser-induced mice without treatment (n ≥ 6 mice/group). **P < 0.01. Error bars correspond to SEM.* ***h*** *Modification of the lipoprotein profile at day 7 after DCA treatment (n ≥ 6 mice/group).* ***i*** *Modification of the lipoprotein profile at day 7 after Avastin treatment. Fraction 1 is mainly composed of VLDL while fraction 5 is mainly composed of HDL*

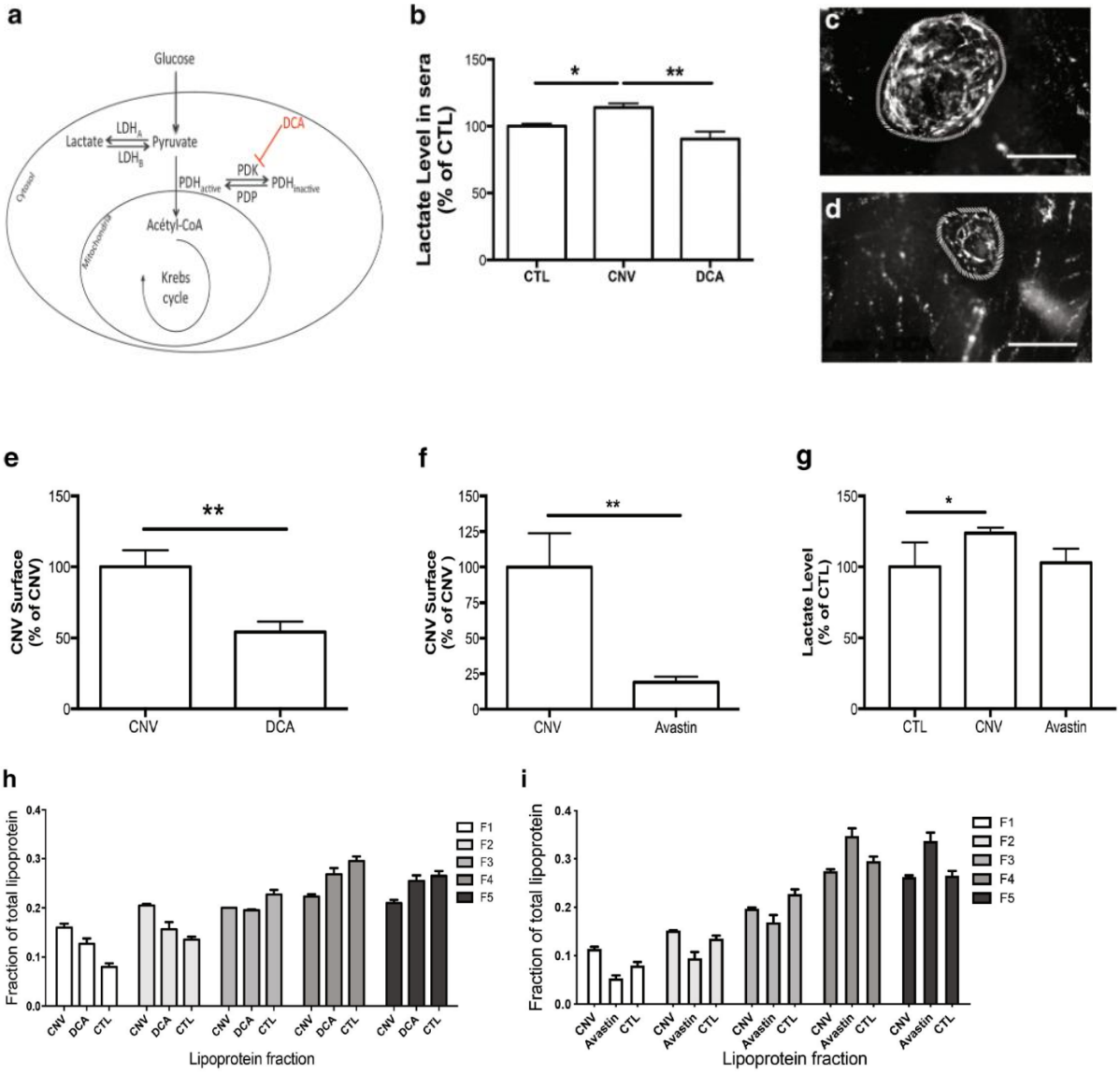
a
Glucose
Lactate
LDH$_A$
LDH$_B$
Pyruvate
DCA
PDK
PDP
PDH$_{active}$
PDH$_{inactive}$
Cytosol
Mitochondria
Acétyl-CoA
Krebs cycle
b
Lactate Level in sera (% of CTL)
150
100
50
0
*
**
CTL
CNV
DCA
c
d
e
CNV Surface (% of CNV)
150
100
50
0
**
CNV
DCA
f
CNV Surface (% of CNV)
150
125
100
75
50
25
0
**
CNV
Avastin
g
Lactate Level (% of CTL)
150
100
50
0
*
CTL
CNV
Avastin
h
Fraction of total lipoprotein
0.4
0.3
0.2
0.1
0.0
F1
F2
F3
F4
F5
CNV DCA CTL CNV DCA CTL CNV DCA CTL CNV DCA CTL CNV DCA CTL
Lipoprotein fraction
i
Fraction of total lipoprotein
0.4
0.3
0.2
0.1
0.0
F1
F2
F3
F4
F5
CNV Avastin CTL CNV Avastin CTL CNV Avastin CTL CNV Avastin CTL CNV Avastin CTL
Lipoprotein fraction

Fig. 4 *Lactate mediates the recruitment of inflammatory cells during CNV. Mice subjected to laser-induced CNV were treated or not with DCA (3 mg DCA/day/mouse). NMR dosage of the lactate level at day 3 and day 5 in eye (**a**), bone marrow (**b**), spleen (**c**), and liver (**d**) (n ≥ 5 mice/group). *P < 0.05; **P < 0.01; ***P < 0.001; ****P < 0.0001; data are expressed as the mean ± SD. Immunostaining of neutrophils (**e–i**) and macrophages (**j–n**) on flat-mounted choroids collected at day 1 (D1: **e, j**), day 3 (D3: **f, k**), day 5 (D5: **g, l**), and day 7 (D7: **h, m**) after laser induction. Scale bars, 100 µm. Dashed lines delineate the lesion. Macrophage/neutrophil density defined as the volume occupied by cells divided by the total laser impact volume with or without treatment with DCA (**i, n**). Percentage of M2 macrophages among CD45⁺ cells determined by flow cytometry (n = 9 eyes/group) (**o**). CTL corresponds to mice not subjected to laser burn. Boyden chamber assay showing the differential migration of human macrophages polarized in vitro into the M1 (**p**) or M2 (**q**) subtype (n = 6 wells/condition).M1 cells were attracted by high and M2 by low-lactate concentrations. Rdm corresponds to random cell migration in the absence of chemoattractant and CTL>O to cell migration in response to BSA-containing medium (positive control). Cultures of M1 macrophages were treated or not with 10 mM lactate for 48 h (**r**). The results obtained after phenotypic analysis showed that lactate induced the conversion of M1 into M2 macrophages (n = 5). *P < 0.05; **P < 0.01; ***P < 0.001; ns, nonsignificant. Data are expressed as the mean ± SEM (**i, n, o**) or mean ± SD (**p, q**). See also Fig. S1 for the gating strategy used in FACS analyses to identify the M2 macrophage subset in posterior eye segments after laser-induced CNV*

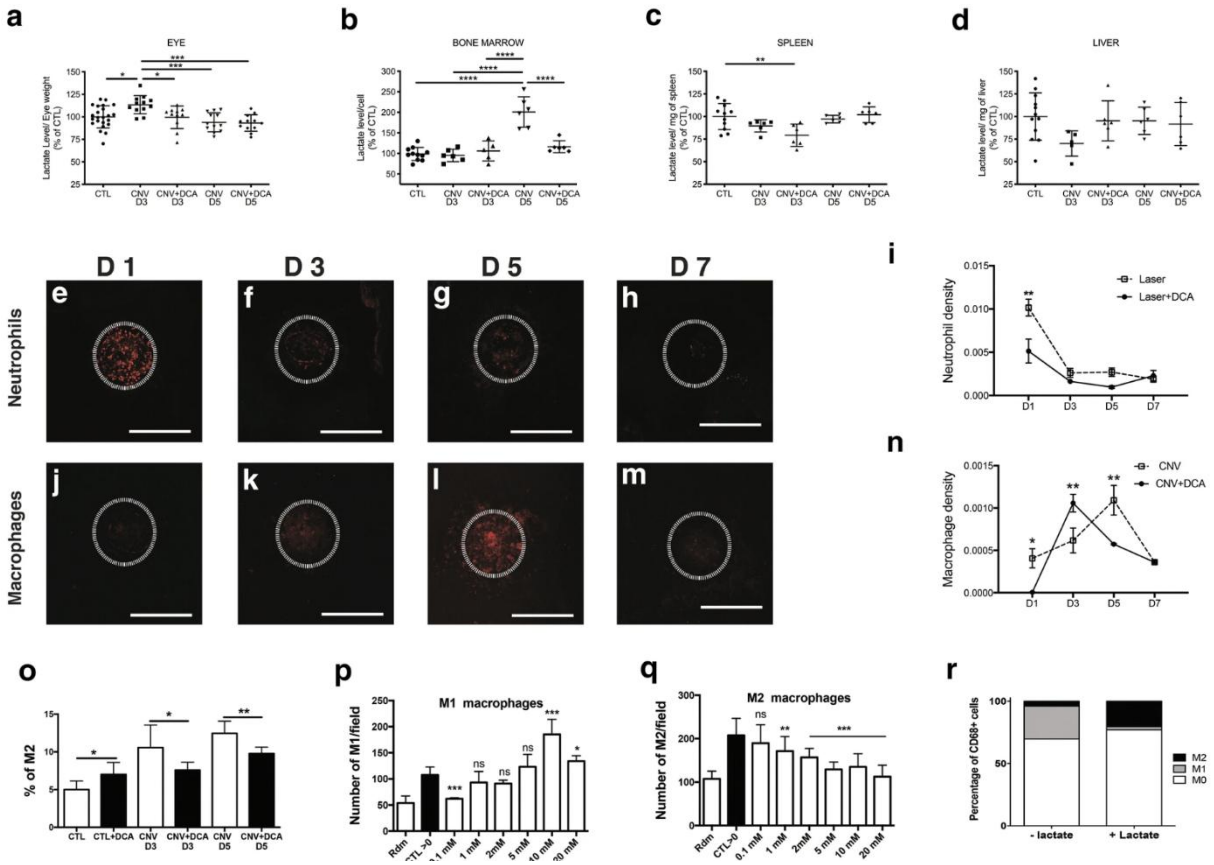

Fig. 5 *DCA treatment during the angiogenic phase of CNV formation is as efficient as anti-VEGF treatment in the murine model.* ***a*** *Summary diagram of the kinetics of inflammation (neutrophils and macrophages), CNV formation, and lactate levels in eyes and sera.* ***b*** *The schedules of DCA treatment (3 mg DCA/day/mouse) are indicated below.* ***c*** *Quantification of fluorescent neovessel area (n ≥ 5 mice/group) showing the maximal reduction of CNV development obtained with the DCA treatments applied from day 0 to day 7 or from day 4 to day 7. The results are expressed as the percentage of laser-induced mice. *P < 0.05; ***P < 0.001; ns, nonsignificant. Error bars are SEM*

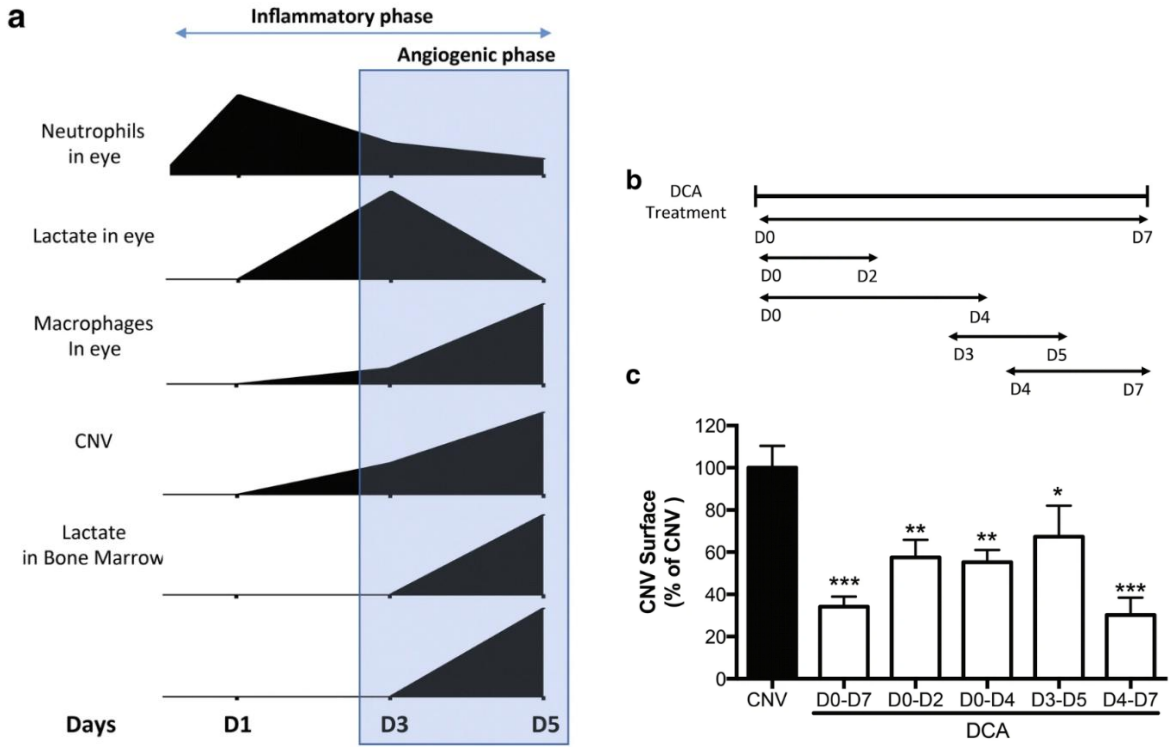

References

1. *Colijn JM, Buitendijk GHS, Prokofyeva E, Alves D, Cachulo ML, Khawaja AP, Cougnard-Gregoire A, Merle BMJ, Korb C, Erke MG, Bron A, Anastasopoulos E, Meester-Smoor MA, Segato T, Piermarocchi S, de Jong PTVM, Vingerling JR, Topouzis F, Creuzot-Garcher C, Bertelsen G, Pfeiffer N, Fletcher AE, Foster PJ, Silva R, Korobelnik J-F, Delcourt C, Klaver CCW, EYERISK consortium, European Eye Epidemiology (E3) consortium (2017) Prevalence of age-related macular degeneration in Europe: the past and the future. Ophthalmology 124:1753–1763*
2. *Schmidt-Erfurth U, Klimscha S, Waldstein SM, Bogunović H (2017) A view of the current and future role of optical coherence tomography in the management of age-related macular degeneration. Eye (Lond) 31:26–44*
3. *Lai T-T, Hsieh Y-T, Yang C-M, Ho T-C, Yang C-H (2019) Biomarkers of optical coherence tomography in evaluating the treatment outcomes of neovascular age-related macular degeneration: a real-world study. Sci Rep 9. https://doi.org/10.1038/s41598018-36704-6,*
4. *Cascella R, Strafella C, Caputo V, Errichiello V, Zampatti S, Milano F, Potenza S, Mauriello S, Novelli G, Ricci F, Cusumano A, Giardina E (2018) Towards the application of precision medicine in age-related macular degeneration. Prog Retin Eye Res 63: 132–146*
5. *DeAngelis MM, Owen LA, Morrison MA, Morgan DJ, Li M, Shakoor A, Vitale A, Iyengar S, Stambolian D, Kim IK, Farrer LA (2017) Genetics of age-related macular degeneration (AMD). Hum Mol Genet 26:R45–R50*
6. *Liu K, Chen LJ, Lai TY, Tam PO, Ho M, Chiang SW, Liu DT, Young AL, Yang Z, Pang CP (2014) Genes in the high-density lipoprotein metabolic pathway in age-related macular degeneration and polypoidal choroidal vasculopathy. Ophthalmology 121:911– 916*
7. *Nita M, Grzybowski A, Ascaso FJ, Huerva V (2014) Age-related macular degeneration in the aspect of chronic low-grade inflammation (pathophysiological parainflammation). Mediat Inflamm 2014: 930671–930610*
8. *Lavalette S, Raoul W, Houssier M, Camelo S, Levy O, Calippe B, Jonet L, Behar-Cohen F, Chemtob S, Guillonneau X, Combadiere C, Sennlaub F (2011) Interleukin-1beta inhibition prevents choroidal neovascularization and does not exacerbate photoreceptor degeneration. Am J Pathol 178:2416–2423*
9. *Doyle SL, Ozaki E, Brennan K, Humphries MM, Mulfaul K, Keaney J, Kenna PF, Maminishkis A, Kiang AS, Saunders SP, Hams E, Lavelle EC, Gardiner C, Fallon PG, Adamson P, Humphries P, Campbell M (2014) IL-18 attenuates experimental choroidal neovascularization as a potential therapy for wet age-related macular degeneration. Sci Transl Med 6:230ra44*
10. *Xi H, Katschke KJ Jr, Li Y, Truong T, Lee WP, Diehl L, Rangell L, Tao J, Arceo R, Eastham-Anderson J, Hackney JA, Iglesias A, Cote-Sierra J, Elstrott J, Weimer RM, Campagne MV (2016) IL33 amplifies an innate immune response in the degenerating retina. J Exp Med 213:189–207*
11. *Colijn JM, den Hollander AI, Demirkan A, Cougnard-Grégoire A, Verzijden T, Kersten E, Meester-Smoor MA, Merle BMJ, Papageorgiou G, Ahmad S, Mulder MT, Costa MA, Benlian P, Bertelsen G, Bron AM, Claes B, Creuzot-Garcher C, Erke MG, Fauser S, Foster PJ, Hammond CJ, Hense H-W, Hoyng CB, Khawaja AP, Korobelnik J-F, Piermarocchi S, Segato T, Silva R, Souied EH, Williams KM, van Duijn CM, Delcourt C, Klaver CCW, Acar N, Altay L, Anastosopoulos E, Azuara-Blanco A, Berendschot T,*

Berendschot T, Bergen A, Bertelsen G, Binquet C, Bird A, Bobak M, Larsen MB, Boon C, Bourne R, Brétillon L, BroeR, Bron A, Buitendijk G, CachuloML, CapuanoV, Carrière I, Chakravarthy U, Chan M, Chang P, Colijn J, Cougnard-Grégoire A, Cree A, Creuzot-Garcher C, Cumberland P, Cunha-Vaz J, Daien V, De Jong E, Deak G, Delcourt C, Delyfer M-N, den Hollander A, Dietzel M, Erke MG, Faria P, Farinha C, Fauser S, Finger R, Fletcher A, Foster P, Founti P, Gorgels T, Grauslund J, Grus F, Hammond C, Heesterbeek T, Hense H-W, Hermann M, Hoehn R, Hogg R, Holz F, Hoyng C, Jansonius N, Janssen S, de Jong E, Khawaja A, Klaver C, Korobelnik J-F, Lamparter J, Le Goff M, Lehtimäki T, Leung I, Lotery A, Mauschitz M, Meester M, Merle B, Meyer zu Westrup V, Midena E, Miotto S, Mirshahi A, MohanSaïd S, Mueller M, Muldrew A, Murta J, Nickels S, Nunes S, Owen C, Peto T, Pfeiffer N, Piermarocchi S, Prokofyeva E, Rahi J, Raitakari O, Rauscher F, Ribeiro L, Rougier M-B, Rudnicka A, Sahel J, Salonikiou A, Sanchez C, Schick T, SchmitzValckenberg S, Schuster A, Schweitzer C, Segato T, Shehata J, Silva R, Silvestri G, Simader C, Souied E, Speckauskas M, Springelkamp H, Tapp R, Topouzis F, van Leeuwen E, Verhoeven V, Verzijden T, Vingerling H, Von Hanno T, Williams K, Wolfram C, Yip J, Zerbib J, Ajana S, ArangoGonzalez B, Arndt V, Bhatia V, Bhattacharya SS, Biarnés M, Borrell A, Bühren S, Calado SM, Colijn JM, Cougnard-Grégoire A, Dammeier S, de Jong EK, De la Cerda B, Delcourt C, den Hollander AI, Diaz-Corrales FJ, Diether S, Emri E, Endermann T, Ferraro LL, Garcia M, Heesterbeek TJ, Honisch S, Hoyng CB, Kersten E, Kilger E, CCW K, Langen H, Lengyel I, Luthert P, Maugeais C, Meester-Smoor M, BMJ MI, Monés J, Nogoceke E, Peto T, Pool FM, Rodríguez E, Ueffing M, Ulrich Bartz-Schmidt KU, van Leeuwen EM, Verzijden T, Zumbansen M (2019) Increased high-density lipoprotein levels associated with age-related macular degeneration. Ophthalmology 126:393–406

12. *Noel A, Jost M, Lambert V, Lecomte J, Rakic JM (2007) Antiangiogenic therapy of exudative age-related macular degeneration: current progress and emerging concepts. Trends Mol Med 13:345–352*
13. *Cheung GCM, Lai TYY, Gomi F, Ruamviboonsuk P, Koh A, Lee WK (2017) Anti-VEGF therapy for neovascular AMD and polypoidal choroidal vasculopathy. Asia Pac J Ophthalmol (Phila) 6:527–534*
14. *Nagai N, Suzuki M, Uchida A, Kurihara T, Kamoshita M, Minami S, Shinoda H, Tsubota K, Ozawa Y (2016) Non-responsiveness to intravitreal aflibercept treatment in neovascular age-related macular degeneration: implications of serous pigment epithelial detachment. Sci Rep 6:29619*
15. *Sun X, Yang S, Zhao J (2016) Resistance to anti-VEGF therapy in neovascular age-related macular degeneration: a comprehensive review. DDDT 1857. https://doi.org/10.2147/DDDT.S97653*
16. *Schmidt-Erfurth U, Chong V, Loewenstein A, Larsen M, Souied E, Schlingemann R, Eldem B, Mones J, Richard G, Bandello F (2014) Guidelines for the management of neovascular age-related macular degeneration by the European Society of Retina Specialists (EURETINA). Br J Ophthalmol 98:1144–1167*
17. *Frédérich M, Pirotte B, Fillet M, de Tullio P (2016) Metabolomics as a challenging approach for medicinal chemistry and personalized medicine. J Med Chem 59:8649–8666*
18. *Beger RD, Dunn W, Schmidt MA, Gross SS, Kirwan JA, Cascante M, Brennan L, Wishart DS, Oresic M, Hankemeier T, Broadhurst DI, Lane AN, Suhre K, Kastenmüller G, Sumner SJ, Thiele I, Fiehn O, Kaddurah-Daouk R, for "Precision Medicine and Pharmacometabolomics Task Group"-Metabolomics Society Initiative (2016) Metabolomics enables precision medicine: "a white paper, community perspective". Metabolomics 12:149*

19. *Li B, He X, Jia W, Li H (2017) Novel applications of metabolomics in personalized medicine: a mini-review. Molecules 22. https://doi. org/10.3390/molecules22071173*
20. *Draoui N, de Zeeuw P, Carmeliet P (2017) Angiogenesis revisited from a metabolic perspective: role and therapeutic implications of endothelial cell metabolism. Open Biol 7:170219*
21. *Mills E, O'Neill LAJ (2014) Succinate: a metabolic signal in inflammation. Trends Cell Biol 24:313–320*
22. *Brown CN, Green BD, ThompsonRB, den Hollander AI, Lengyel I (2019) Metabolomics and age-related macular degeneration. Metabolites 9. https://doi.org/10.3390/metabo9010004*
23. *Luo D, Deng T, Yuan W, Deng H, Jin M (2017) Plasma metabolomic study in Chinese patients with wet age-related macular degeneration. BMC Ophthalmol 17:165*
24. *Mitchell SL, Uppal K, Williamson SM, Liu K, Burgess LG, Tran V, Umfress AC, Jarrell KL, Cooke Bailey JN, Agarwal A, PericakVance M, Haines JL, Scott WK, Jones DP, Brantley MA (2018) The carnitine shuttle pathway is altered in patients with neovascular age-related macular degeneration. Invest Ophthalmol Vis Sci 59: 4978–4985*
25. *Osborn MP, Park Y, Parks MB, Burgess LG, Uppal K, Lee K, Jones DP, Brantley MA Jr (2013) Metabolome-wide association study of neovascular age-related macular degeneration. PLoS One 8:e72737*
26. *Laíns I, Duarte D, Barros AS, Martins AS, Gil J, Miller JB, Marques M, Mesquita T, Kim IK, Cachulo M d L, Vavvas D, Carreira IM, Murta JN, Silva R, Miller JW, Husain D, Gil AM (2017) Human plasma metabolomics in age-related macular degeneration (AMD) using nuclear magnetic resonance spectroscopy. PLoS One 12:e0177749*
27. *Lambert V, Lecomte J, Hansen S, Blacher S, Gonzalez ML, Struman I, Sounni NE, Rozet E, de Tullio P, Foidart JM, Rakic JM, Noel A (2013) Laser-induced choroidal neovascularization model to study age-related macular degeneration in mice. Nat Protoc 8:2197–2211*
28. *Adeva M, González-Lucán M, Seco M, Donapetry C (2013) Enzymes involved in l-lactate metabolism in humans. Mitochondrion 13:615–629*
29. *Roche TE, Hiromasa Y (2007) Pyruvate dehydrogenase kinase regulatory mechanisms and inhibition in treating diabetes, heart ischemia, and cancer. Cell Mol Life Sci 64:830–849*
30. *Bian L, Josefsson E, Jonsson IM, Verdrengh M, Ohlsson C, Bokarewa M, Tarkowski A, Magnusson M (2009) Dichloroacetate alleviates development of collagen II-induced arthritis in female DBA/1 mice. Arthritis Res Ther 11:R132*
31. *Matheus N, Hansen S, Rozet E, Peixoto P, Maquoi E, Lambert V, Noel A, Frederich M, Mottet D, de Tullio P (2014) An easy, convenient cell and tissue extraction protocol for nuclear magnetic resonance metabolomics. Phytochem Anal: PCA 25:342–349*
32. *Sounni NE, Cimino J, Blacher S, Primac I, Truong A, Mazzucchelli G, Paye A, Calligaris D, Debois D, De Tullio P, Mari B, De Pauw E, Noel A (2014) Blocking lipid synthesis overcomes tumor regrowth and metastasis after antiangiogenic therapy withdrawal. Cell Metab 20:280–294*
33. *Mia S, Warnecke A, Zhang X-M, Malmström V, Harris RA (2014) An optimized protocol for human M2 macrophages using M-CSF and IL-4/IL-10/TGF- β yields a dominant immunosuppressive phenotype. Scand J Immunol 79:305–314*

34. *Edin S, Wikberg ML, Rutegård J, Oldenborg P-A, Palmqvist R (2013) Phenotypic skewing of macrophages in vitro by secreted factors from colorectal cancer cells. PLoS One 8:e74982. https://doi.org/10.1371/journal.pone.0074982*
35. *Hubert P, van den Brûle F, Giannini SL, Franzen-Detrooz E, Boniver J, Delvenne P (1999) Colonization of in vitro-formed cervical human papillomavirus-associated (pre)neoplastic lesions with dendritic cells. Am J Pathol 154:775–784*
36. *Pennesi ME, Neuringer M, Courtney RJ (2012) Animal models of age-related macular degeneration. Mol Asp Med 33:487–509*
37. *Michelakis ED, Webster L, Mackey JR (2008) Dichloroacetate (DCA) as a potential metabolic-targeting therapy for cancer. Br J Cancer 99:989–994*
38. *Kersten E, Paun CC, Schellevis RL, Hoyng CB, Delcourt C, Lengyel I, Peto T, Ueffing M, Klaver CCW, Dammeier S, den Hollander AI, de Jong EK (2018) Systemic and ocular fluid compounds as potential biomarkers in age-related macular degeneration. Surv Ophthalmol 63:9–39*
39. *Porporato PE, Payen VL, De Saedeleer CJ, Préat V, Thissen J-P, Feron O, Sonveaux P (2012) Lactate stimulates angiogenesis and accelerates the healing of superficial and ischemic wounds in mice. Angiogenesis 15:581–592*
40. *Beckert S, Farrahi F, Aslam RS, Scheuenstuhl H, Konigsrainer A, Hussain MZ, Hunt TK (2006) Lactate stimulates endothelial cell migration. Wound Repair Regen 14:321–324*
41. *Skeie JM, Mullins RF (2009) Macrophages in neovascular age-related macular degeneration: friends or foes? Eye (Lond) 23: 747–755*
42. *Sakurai E, Anand A, Ambati BK, van Rooijen N, Ambati J (2003) Macrophage depletion inhibits experimental choroidal neovascularization. Invest Ophthalmol Vis Sci 44:3578–3585*
43. *Zandi S, Nakao S, Chun KH, Fiorina P, Sun D, Arita R, Zhao M, Kim E, Schueller O, Campbell S, Taher M, Melhorn MI, Schering A, Gatti F, Tezza S, Xie F, Vergani A, Yoshida S, Ishikawa K, Yamaguchi M, Sasaki F, Schmidt-Ullrich R, Hata Y, Enaida H, Yuzawa M, Yokomizo T, Kim YB, Sweetnam P, Ishibashi T, Hafezi-Moghadam A (2015) ROCK-isoform-specific polarization of macrophages associated with age-related macular degeneration. Cell Rep 10:1173–1186*
44. *Jetten N, Verbruggen S, Gijbels MJ, Post MJ, De Winther MPJ, Donners MMPC (2014) Anti-inflammatory M2, but not proinflammatory M1 macrophages promote angiogenesis in vivo. Angiogenesis 17:109–118*
45. *Colegio OR, Chu NQ, Szabo AL, Chu T, Rhebergen AM, Jairam V, Cyrus N, Brokowski CE, Eisenbarth SC, Phillips GM, Cline GW, Phillips AJ, Medzhitov R (2014) Functional polarization of tumour-associated macrophages by tumour-derived lactic acid. Nature 513:559–563*
46. *Dhup S, Dadhich RK, Porporato PE, Sonveaux P (2012) Multiple biological activities of lactic acid in cancer: influences on tumor growth, angiogenesis and metastasis. Curr Pharm Des 18:1319– 1330*
47. *Hurley JB, Lindsay KJ, Du J (2015) Glucose, lactate, and shuttling of metabolites in vertebrate retinas. J Neurosci Res 93:1079–1092*
48. *De Bock K, Georgiadou M, Schoors S, Kuchnio A, Wong BW, Cantelmo AR, Quaegebeur A, Ghesquiere B, Cauwenberghs S, Eelen G, Phng LK, Betz I, Tembuyser B, Brepoels K, Welti J, Geudens I, Segura I, Cruys B, Bifari F, Decimo I, Blanco R, Wyns S, Vangindertael J, Rocha S, Collins RT, Munck S, Daelemans D, Imamura H, Devlieger R, Rider M, Van Veldhoven PP, Schuit F, Bartrons R, Hofkens J,*

Fraisl P, Telang S, Deberardinis RJ, Schoonjans L, Vinckier S, Chesney J, Gerhardt H, Dewerchin M, Carmeliet P (2013) Role of PFKFB3-driven glycolysis in vessel sprouting. Cell 154:651–663

49. *Parmeggiani F, Romano MR, Costagliola C, Semeraro F, Incorvaia C, D'Angelo S, Perri P, De Palma P, De Nadai K, Sebastiani A (2012) Mechanism of inflammation in age-related macular degeneration. Mediat Inflamm 2012:546786–546716*
50. *Brizel DM, Schroeder T, Scher RL, Walenta S, Clough RW, Dewhirst MW, Mueller-Klieser W (2001) Elevated tumor lactate concentrations predict for an increased risk of metastases in head-and-neck cancer. Int J Radiat Oncol Biol Phys 51:349–353*
51. *Quennet V, Yaromina A, Zips D, Rosner A, Walenta S, Baumann M, Mueller-Klieser W (2006) Tumor lactate content predicts for response to fractionated irradiation of human squamous cell carcinomas in nude mice. Radiother Oncol 81:130–135*